doi:10.1093/brain/awn270 *Brain* (2008), **131**, 3395–3409

Subthalamic nucleus functional organization revealed by parkinsonian neuronal oscillations and synchrony

A. Moran,[1] H. Bergman,[2] Z. Israel[3] and I. Bar-Gad[1,4]

[1]Gonda Multidisciplinary Brain Research Center, Bar Ilan University, Ramat Gan, [2]Department of Physiology, Hadassah Medical School and Interdisciplinary Center for Neural Computation, The Hebrew University, Jerusalem, [3]Department of Neurosurgery, Hadassah University Hospital, Jerusalem and [4]Goodman Faculty of Life Sciences, Bar Ilan University, Ramat Gan, Israel

Correspondence to: Anan Moran, Gonda Multidisciplinary Brain Research Center, Bar Ilan University, Ramat-Gan, Israel
E-mail: anan.moran@live.biu.ac.il

The emergence of oscillations and synchrony among neurons of the basal ganglia is a well-known characteristic of Parkinson's disease. In this study we used intra-operative microelectrode recording to investigate this inter-relationship between these two phenomena in the subthalamic nucleus (STN) neurons of 39 human Parkinson's disease patients undergoing deep brain stimulation surgery. From the recorded neuronal traces both neuronal spike trains and their background activity were extracted, and their spectral characteristics were evaluated. We have used the background oscillations as a marker for synchronized activity in the local population in the neuron vicinity and studied its relation to single neuron oscillations. Spike train background oscillations were evaluated using a procedure of background reconstruction that consisted of spikes removal from the original traces and full wave rectification followed by standard spectral analysis. Coherence and phase analysis between oscillatory spike trains and their oscillatory background were also conducted to study the phase relationship between the two. Of the 231 neuronal spike-trains which were sorted offline, 82 (35%) showed significant oscillatory activity. These neurons were found to oscillate mostly in two bands; 3–7 Hz, termed the Tremor Frequency Band (TFB), and 8–20 Hz, termed the High-Frequency Band (HFB). While HFB neurons oscillated for longer periods and always coherently with their background activity, TFB neurons oscillated more episodically and only a half were coherent with their background. These findings indicate that the two neuronal populations are the outcome of very different oscillatory drives deriving from different local functional neuronal organizations.

Keywords: Parkinson's disease; subthalamic nucleus; oscillations; neural synchronization; microelectrode recording; human

Abbreviations: DBS = deep brain stimulation; DFB = dual frequency band; HFB = high-frequency band; HiBB = high beta band; LFP = local field potentials; MPTP = 1-methyl 4-phenyl 1,2,3,6-tetrahydropyridine; PR = power ratio; PSD = power spectral density; RMS = root mean square; STN = subthalamic nucleus; TFB = tremor frequency band

Received June 4, 2008. Revised August 18, 2008. Accepted September 22, 2008. Advance Access publication November 4, 2008

Introduction

Periodic oscillations play a cardinal role in the normal functioning of the nervous system (Engel *et al.*, 1999; Pare *et al.*, 2002; Buzsaki 2006). In addition to their normal expression, pathological oscillations have also been found in several cognitive and motor disorders such as epilepsy and Parkinson's disease. In Parkinson's disease, oscillations have primarily been explored to find physiological correlates of the observed rest tremor (Schwab and Cobb 1939; Lenz *et al.*, 1988; Hutchison *et al.*, 1997), one of the hallmark symptoms of the disease. Tremor-related 3–7 Hz oscillations have indeed been found in the central nervous system of Parkinson's disease patients and in the 1-methyl 4-phenyl 1,2,3,6-tetrahydropyridine (MPTP) primate model of the disease in several brain regions including the motor cortex (Volkmann *et al.*, 1996; Timmermann *et al.*, 2002), thalamus (Zirh *et al.*, 1998) and several nuclei of the basal ganglia (Bergman *et al.*, 1994; Raz *et al.*, 2000; Levy *et al.*, 2001). Some studies have found a direct relation between basal ganglia oscillations and tremor (Hutchison *et al.*, 1997; Amtage *et al.*, 2008), while others have not found coherence between the two physiological phenomena over longer time spans (Lemstra *et al.*, 1999; Raz *et al.*, 2000; Hurtado *et al.*, 2005), suggesting a more complex, non-linear relationship between them.

Several groups looking at data from human Parkinson's disease patients and from the primate MPTP model have reported a broad range of abnormal oscillations apart from

low-frequency tremor-related ones, such as in the alpha (8–13 Hz) (Bergman *et al.*, 1994; Raz *et al.*, 2000), beta (15–30 Hz) (Brown *et al.*, 2001; Cassidy *et al.*, 2002; Levy *et al.*, 2002*b*; Priori *et al.*, 2002) and gamma (30–100 Hz) (Brown *et al.*, 2001; Cassidy *et al.*, 2002) frequency bands. Further support for a relationship between these oscillations and the pathological state comes from studies showing a reduction in the amplitude of these oscillations in conjunction with reduced tremor scores following pharmacological intervention (Brown *et al.*, 2001; Levy *et al.*, 2002*a*; Priori *et al.*, 2004), cortical and subthalamic nucleus (STN) electrical stimulation (Drouot *et al.*, 2004; Wingeier *et al.*, 2006) and even active movement of the limbs (Cassidy *et al.*, 2002; Levy *et al.*, 2002*a*; Amirnovin *et al.*, 2004; Kuhn *et al.*, 2004).

This increased oscillatory activity is accompanied by a dramatically higher correlation in spike firing across neurons of the basal ganglia (Raz *et al.*, 1996; Levy *et al.*, 2000). This increase in correlated activity has been hypothesized to be part of a segregation loss between parallel information pathways flowing through the basal ganglia (Alexander *et al.*, 1986; Middleton and Strick, 2002; Pessiglione *et al.*, 2005). The loss of segregated information flow leads to reduced specificity of the action selection process. This loss of a winning motor program presumably gives rise to the hypokinetic symptoms of Parkinson's disease such as akinesia and bradykinesia (Alexander and Crutcher, 1990; Mink, 1996).

Oscillations and synchrony are both evident in the parkinsonian state, but their relation is unclear. Some studies have reported a strong relation between the two phenomena. These include the oscillatory correlation of basal ganglia neurons (Raz *et al.*, 2000; Levy *et al.*, 2002*b*) and the coherence of single neurons with the local field potential (LFP) (Goldberg *et al.*, 2004; Weinberger *et al.*, 2006), whereas other studies suggest that they manifest separately (Heimer *et al.*, 2002). In this study we investigated the relationship between single neuron oscillations and synchronicity within its local neuronal neighbourhood. This was done by analyzing the relationship between single neuron spike trains and their background oscillatory activity using micro electrode recording from the STN of Parkinson's disease patients during deep brain stimulation (DBS) surgery. The recorded high-pass filtered background activity reflects the sum of the local population neuronal spiking activity in the vicinity of the electrode. Thus, it can capture the network's co-activation levels and frequencies, bridging the gap between single-cell oscillations and neural population synchrony.

Methods

Patients

The data were collected from 71 STNs of 39 Parkinson's disease patients aged 43–74 years (59 ± 7, all statistics presented in this article use mean ± standard deviation notation, unless otherwise stated), undergoing DBS surgery for implantation of stimulating electrodes for the treatment of Parkinson's disease. Individual information regarding the patients is provided in Supplementary Table 1. The patients were assessed preoperatively using the Unified Parkinson's Disease Rating Scale (UPDRS) in the 'off' state. In addition to the total UPDRS score, three aggregative scores reflecting tremor, rigidity and bradykinesia were attributed to each of the patients. Tremor and rigidity scores are each calculated as the sum of all tremor and rigidity UPDRS sub-scores, respectively (maximum of 28 for tremor and 20 for rigidity). The bradykinesia score is the sum of the UPDRS sub-sections for facial expression, finger taps, hand movements, pronation–supination of the hands, leg agility, arising from chair and body bradykinesia (maximum of 44). The 'off' scores were unavailable for seven patients and thus 32 patients were included in the clinical statistics analysis. All patients signed a written informed consent for the surgery that involved microelectrode recording. Use of the data in this research was approved by the ethics committee of Hadassah University Hospital, Jerusalem, Israel. Patients underwent psychological and neurological assessment and met all the standard criteria for STN DBS surgery (Lang and Widner 2002; Machado *et al.*, 2006).

Surgery and data acquisition

The STN target was initially identified on a T_1 or T_2 MR image. Trajectory planning was performed after fusing the MRI with a stereotactic CT image using Framelink^{TM} software (Medtronic, Minneapolis, MN). Microelectrode recordings were performed for STN localization prior to implantation of a chronic stimulating electrode as described in detail previously (Moran *et al.*, 2006). Briefly, via a frontal burr hole, one or two polyimide-coated tungsten microelectrodes (Frederick Haer, Bowdoinham, ME and AlphaOmega Engineering, Nazareth, Israel, impedance 0.58 ± 0.2 MΩ at 1000 Hz) were advanced towards the target in adjustable sub-millimeters steps. STN border localization was determined by an expert neurophysiologist intra-operatively by inspecting the microelectrode recorded traces. Intra-operative macro-stimulation further confirmed STN location and absence of stimulation induced side-effects. A permanent stimulating electrode was implanted such that the desired contact was positioned in the centre of the STN on the dorso-ventral axis as defined by the entry and exit points. Postoperative imaging confirmed electrode location to be within the STN. Data acquisition and electrode position control used the MicroGuide system (AlphaOmega Engineering, Nazareth, Israel). Recording sessions began 1 s after movement of the electrode ceased, and stopped with the next movement of the electrode. Recorded signals from the microelectrode were amplified by 10 000 and band-pass filtered between 250 and 6000 Hz using a four-pole Butterworth filter. The signals were then sampled at 48 KHz (occasionally at 24 KHz), by 12-bit A/D converter, with 10 V input range yielding ~0.25 μV amplitude resolution. Patients were awake during the entire recording session, with no administration of anaesthetics or sedative agents. Anti-parkinsonian medications were discontinued at least 12 h prior to surgery.

Data preparation and analysis

Signal stability screening

Data preparation and analysis used MATLAB V7 (Mathworks, Natick, MA). Only recording traces that had passed a two-stage screening test were included in the analysis. First, sessions shorter

than 10 s or containing artefacts with amplitudes exceeding 300 μV were rejected. Second, to test the recorded session stability each session was divided into consecutive one second segments. Each of these 1 s segments was further divided into 50 ms parts, and their root mean square (RMS) value was calculated (yielding 20 RMS values for each 1 s). The variance of the RMS was then calculated for each 1 s segment. Recorded sessions were considered unstable if they failed to pass Bartlett's test for equal variances across all one second segments with $P<0.0001$. These parameters were chosen following visual inspection of the data and division into stable and unstable recordings by a human expert.

Spike train processing

Spike trains were sorted from the recorded traces using Offline Sorter V2.8.4 (Plexon, Denton, TX). Figure 1A presents two 1-s traces of recorded neuronal activity with superimposed spike locations marked by red and green dots. Cells were sorted only from recorded traces confirmed by the expert neurophysiologist to reside within the STN. Only stable, well-isolated single neurons over 18 s long (46 ± 21 s) were processed. Traces with severe cardiac-pulsation induced modulation which interfered with the extraction of stable spike trains were screened out. Isolation of the spike train was graded by evaluating the fraction of spikes within the refractory period of 1.5 ms out of the total number of spikes in the spike train (Fee *et al.*, 1996). Only spike trains with a fraction <0.5% were processed (i.e. multi-unit spike trains were excluded). Firing rate stability was evaluated using 1-s bins over the whole session. A spike train was considered stable if it had roughly retained the same firing rate over the recording period. We used visual criteria rather than statistical criteria (Gourevitch and Eggermont, 2007) due to the low discharge rate of STN neurons and the limited recording duration.

Neural background activity extraction

The spike timestamps found using the offline sorting procedure (Fig. 2A, red dots) were used to reconstruct the background

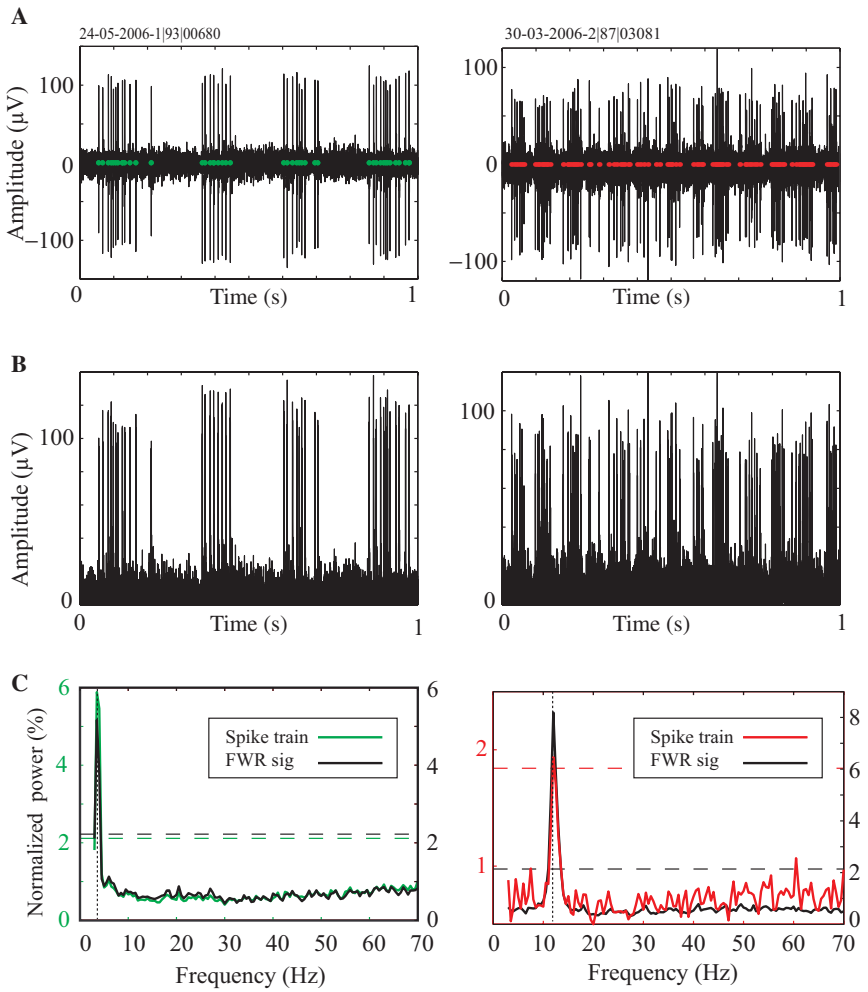

Fig. 1 Calculation method for assessing the main oscillation frequencies in STN single units' spike trains and neuronal population activity. (**A**) Two examples of traces showing oscillating bursting activity. Red and green dots (at zero level) indicate spike timing identified by offline sorting. (**B**) FWR of the traces in (**A**). This method was used in the process of calculating oscillatory bursting activity in the raw traces and the extracted background. (**C**) Normalized PSD of FWR traces in (**B**) after mean subtraction (black), and spike trains in (**A**) (green and red, for the spike trains in (**A**), respectively). Each PSD was normalized by its mean power between 30–70 Hz. Dashed vertical lines indicate the main oscillatory frequency of the spike train. Dashed horizontal lines indicate significance levels of the power of the spike train (coloured) and FWR raw signal (black).

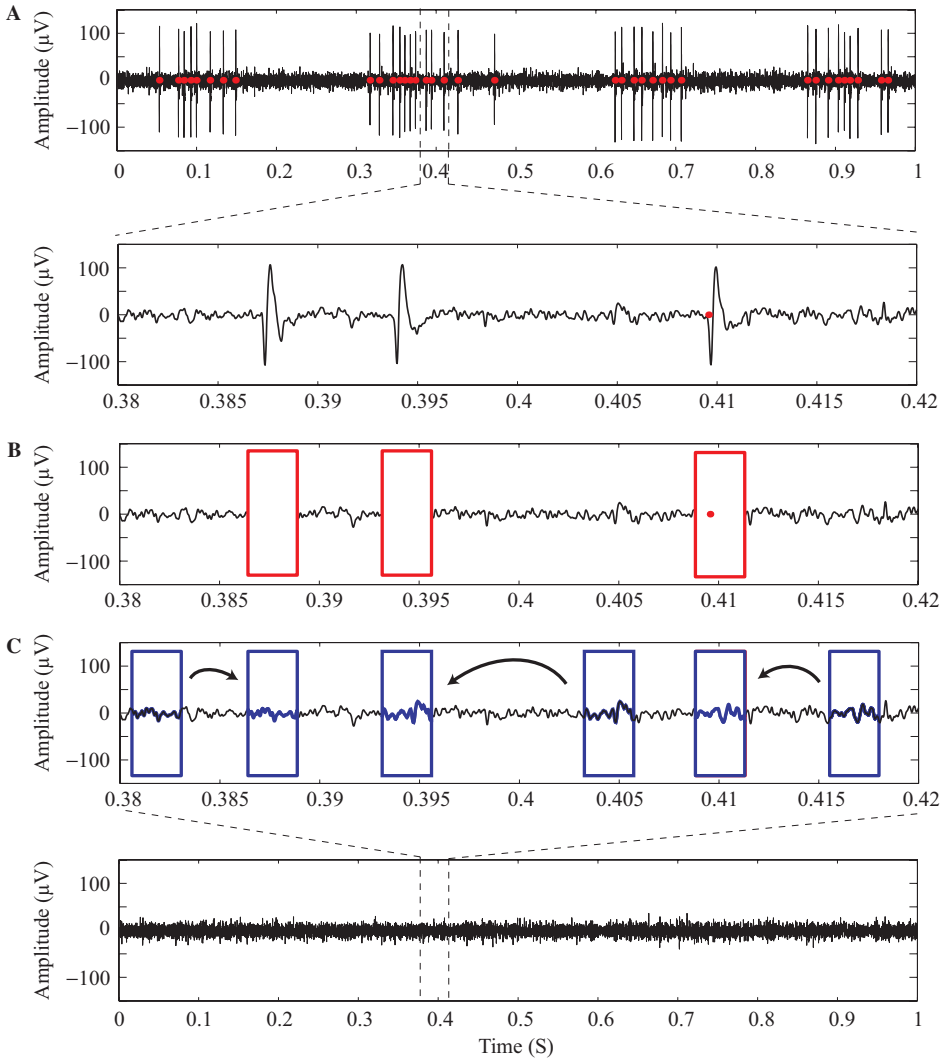

Fig. 2 The procedure for background extraction is demonstrated on a neuron with a main frequency of 4 Hz. (**A**) Timestamps (red dots) taken from the off-line sorting procedure (including unsorted spikes) placed on the raw signal. (**B**) Windows of 0.5 ms before and 2.5 ms after each spike were cleared. (**C**) These empty windows were filled with a consecutive random, spike-free, 3 ms signal from the same trace (blue windows, arrows indicate copy). For illustrative purposes the replacement windows were taken from random areas near the replaced windows. In the real procedure they were taken randomly from the whole spike-free trace. A view of the whole reconstructed background reveals a generally spike-free signal.

activity. In this procedure, the traces in the segments from 0.5 before to 2.5 ms after each spike timestamp (including unsorted spikes) in the raw trace (Fig. 2B) were replaced by a random spike-free 3 ms consecutive signal from a random location within the same recorded trace (Fig. 2C). This reconstructed novel trace (Fig. 2C, bottom) was termed the neuron's 'background activity'. Each extracted background activity signal was visually inspected to confirm that no significant spikes were left, leaving only a few, near-noise level, secondary neurons' spikes.

Power spectrum density estimation of the spike trains

Oscillatory characteristics were assessed using the power spectrum density (PSD) of the spike train with the Welch method (Fig. 1C, coloured lines for the spike trains in Fig. 1A). Its parameters included a Hanning window of a length equal to the number of samples in 2 s, and a 50% overlap between windows that produced a 0.5 Hz spectral resolution. Significant frequencies were considered to be those exceeding a threshold of 5 SD above the mean power in the 30–70 Hz band. For each spike train the 'main oscillation frequency' was defined as the frequency with the maximal power of all the frequencies which exceeded the threshold (Fig 1C, dashed line).

PSD estimation of raw and background traces

The raw recorded traces were online high-pass filtered, leaving only negligible energy in the band of interest (below 70 Hz) that prevented direct inspection of the lower frequency range. Since the background traces were reconstructed from the raw traces they also retain this spectral property. However, the envelope of these traces (both raw and background) contains information regarding low-frequency modulation of the high-frequency activity. Envelope extraction employed full wave rectification (FWR) method

(Journee, 1983; Myers *et al.*, 2003), i.e. analysis of the absolute value of the sampled signal (Fig. 1B for the raw signals in 1A). This was followed by mean subtraction to remove the DC component which was created by the signal rectification [$x_{FWR}(i) = |x(i)| - \langle|x|\rangle$, where x is the original signal]. The Welch method was used for spectral estimation of the FWR traces with the same parameters as for the spike train analysis, leading to a 0.5 Hz resolution. Simulation and verification of this method is found in Supplementary Fig. 1. Significant frequencies and the main oscillation frequency were defined and calculated as for the spike trains (Fig. 1C, black lines). The band surrounding 50 Hz (48–52 Hz) was removed due to occasional high power artefacts in this band.

Spike-to-background power ratio index calculation

The power ratio (PR) index was used to evaluate the difference in saliency of the neuron's main oscillatory frequency between the neuronal spike train and its background activity. To calculate the PR we first calculated the PSD of the neuronal spike train and its background activity. Second, the two PSDs were normalized to enable their comparison. To normalize, each PSD was divided by its total power in the 3–70 Hz band (excluding 48–52 Hz band) to obtain the relative power within the band. Last, the PR index was calculated as the ratio between the normalized power in the background and the raw traces within a 3 Hz sub-band surrounding the main oscillatory frequency of the spike train.

Coherence calculation between spike trains and their background activity

Coherence was used to study the degree of relationship, as function of frequency, between neurons and their background activity. The coherence function is the cross spectral density of the two traces normalized by their auto-spectrums. The coherence values therefore range between 0 and 1, indicating a none to perfect linear phase relationship, respectively. A perfect coherence in a certain frequency requires both signals to have a constant phase relation along the whole recording duration. The frequency resolution was 0.5 Hz, using the same parameters as for the PSD calculations. A significant coherence level was calculated as $limit = 1-(1-\alpha)^{1/(N-1)}$, where $\alpha = 0.99$ and N is the number of 2-s consecutive windows used for coherence calculation (Rosenberg *et al.*, 1989). This significance level gives a confidence value of $P < 0.01$ to reject the null hypothesis of non-significant coherence. Significant coherence was tested for a 3 Hz frequency range surrounding the main oscillation frequency of the spike train. If any of the frequencies in the range were above the significance limit the signal was considered significantly coherent.

Spike train-background phase distribution

We investigated the phase of the neural spike trains relative to the phase of the oscillating background. Following the background signal extraction of traces that produced the spike trains (Fig. 3A), the background was low-pass filtered with a cut-off frequency of 500 Hz, down sampled to ~1 KHz, full wave rectified and mean subtracted. Next the rectified background was band-passed filtered in the specific neuron frequency range corresponding to its spike train group [3–7 Hz FIR bandpass filter for the tremor frequency band (TFB) group, and 8–20 Hz FIR bandpass filter for the High-Frequency Band (HFB) group] (Fig. 3B). All filtering were done twice, in both forward and reverse directions, to ensure zero phase shifts. In order to define oscillation cycles, positive and negative peaks in the filtered background were found. An oscillation cycle was defined between two neighbouring negative peaks (troughs). Half a cycle was defined as the positive peak between the two troughs regardless of its position between the two (Fig. 3C). Next each spike's phase was calculated as its relative location on the half cycle it resided on. The calculation was done on half a cycle resolution to bypass the slightly different lengths of the two cycle halves. After calculating each spike train's spike phases, its phase distribution and mean phase were calculated (Fig. 3D). Deviation from uniform distribution of phases was assessed using a Rayleigh test with $P < 0.001$.

Another method to assess a neuron's preferred phase was carried out by modelling the phase distribution as a cosine function (Fig. 3E). To find the cosine phase an optimal fit was calculated using the function $Y = A*cos(2*\pi*t-\theta) + B$, where A, θ, and B are the amplitude, phase and shift-fitted parameters, respectively. The θ parameter was then defined as the neuron's preferred phase with respect to the peak background activity. A phase of 180° represents a tendency of the neuron to fire together with the peak of the background activity, while higher or lower values mean that spikes tend to occur after or before peak background activity, respectively.

If the population size is infinite, both methods (the direct time calculation of the phase and the cosine modelling) are equivalent and provide the same results (Sanger, 1994). However, a finite sample size may lead to a bias in the estimate. Therefore, we used both methods to provide further support for the main result.

Quantification of the temporal stability of oscillations: the Duration Index

The duration index was defined to quantify the temporal stability of the main oscillatory frequency. It was calculated in two steps. First, a threshold was defined as 5 SD above the mean power between 3–70 Hz (excluding the 48–52 Hz band) of the signal PSD. Second, the spectrogram was calculated using the Welch method with 1-s non-overlapping windows, and 1 Hz spectral resolution. (These are also the parameters of the spectrograms in Figures 6 and 8.) The duration index was defined as the fraction of the total signal time span during which the PSD in a range of 2 Hz above and below the main oscillatory frequency crossed the 5 SD threshold. This procedure was carried out for both spike trains and for the raw FWR signals.

Results

Neural activity was recorded in the STN of 39 Parkinson's disease patients undergoing DBS surgery and processed offline to extract spike trains and for further analysis. Of the 231 spike trains of highly isolated and stable neurons, 82 (35%) showed significant oscillatory activity at least at one frequency. Spectral analysis of the spike trains revealed a bimodal distribution of their main oscillatory frequency with peaks near 4 and 13 Hz (Fig. 4A). The frequency distribution around 4 Hz was narrowly spread between 3 and 7 Hz (4.47 ± 0.71) and was termed the TFB, while the distribution around 13 Hz was wider and ranged from 8 to 20 Hz (12.71 ± 2.37), and was termed the HFB. Example traces of TFB and HFB neuronal activity are presented in Fig. 1A left

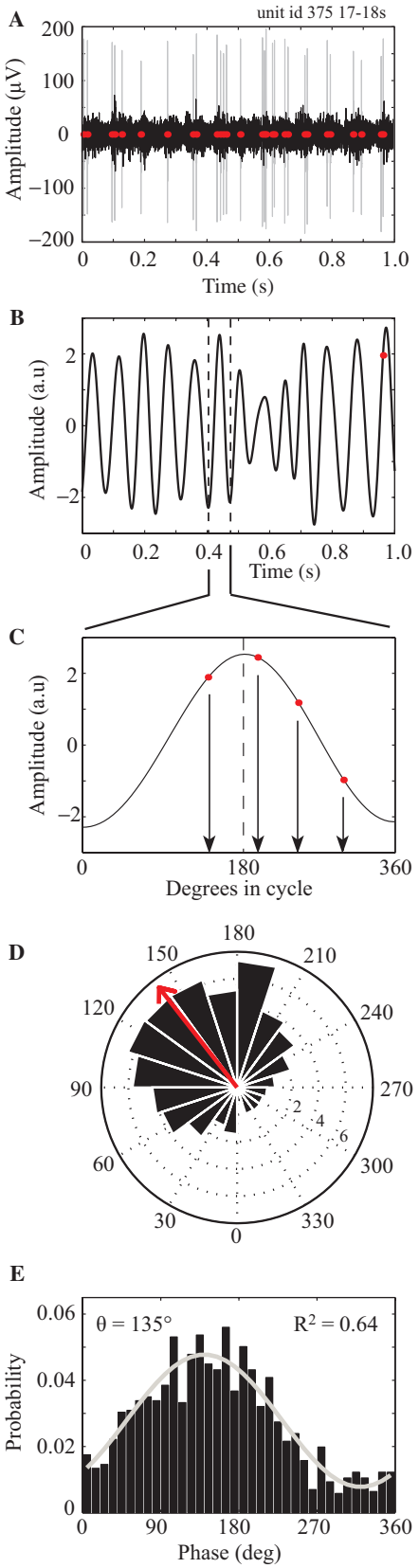

Fig. 3 Phase relation calculation between spike trains and their background. (**A**) Spike train timestamps (red dots) superimposed on raw trace (light grey) and background activity (black). (**B**) Spike train times (red dots) as in (**A**) superimposed on the HFB range (8–20 Hz) band-passed FWR background activity (black). Dashed lines mark the area between two adjacent troughs defined as one cycle (**C**) detail of the single cycle marked in (**B**). Arrows indicate phases of spikes in the cycle. Dashed line marks the peak of cycle which serves as half of cycle. (**D**) Spike phase distribution of the full spike train which one second of it is shown in (**A**). Red arrow represents the mean phase. Scale is the percentage within the total phase population. (**E**) Cosine model fit to the phase distribution for the unit in (**A**). θ is the best fit phase parameter of the cosine model to the phase distribution. In all analyses, peak background is at 180°.

and right, respectively. Neurons with significant oscillations in both frequency ranges were termed Dual Frequency Band (DFB) neurons. Of the 82 neurons with significant oscillatory activity 37 (45%) were TFB neurons, 34 (41%) were HFB neurons and 9 (11%) were DFB neurons. Neurons displaying higher frequencies in the high beta band (HiBB) (only two neurons at around 22 Hz) were not further analysed due to their scarcity. No units were found with a main oscillatory freq >25 Hz. The band below 3 Hz was neglected due to frequent recorded artefacts caused among other things by blood flow and respiration.

A total of 39 patients participated in this study. They demonstrated a broad range and mixture of clinical symptoms reflecting different rigidity, tremor and bradykinesia scores (Supplementary Table 1). Thirty-two patients with available UPDRS scores were divided into four groups according to the types of oscillatory cells recorded during their surgery. The four groups were defined as those with only oscillating TFBs (11 patients), only oscillating HFBs (six patients), those with both HFB and TFB or with DFB (six patients), and finally those with only non-oscillatory cells (nine patients). For each of these groups the mean clinical scores for rigidity, tremor and bradykinesia were calculated (Supplementary Table 2). Kruskal–Wallis non-parametric tests, calculated separately on each of the clinical states revealed no significant differences between the groups with respect to each of the clinical scores.

The firing rates of the TFB, HFB, DFB and non-oscillating neuronal groups were 40.3 ± 12.1, 42.2 ± 16.7, 43.9 ± 8.4 and 30.8 ± 13.2, respectively. The firing rates of the three oscillating groups were not statistically different from each other (unpaired *t*-test, $P > 0.4$), but they were all significantly different from the non-oscillating group (unpaired *t*-test, $P < 0.001$). The distribution of the recorded neurons along the dorso-ventral axis revealed that TFB, HFB and DFB neurons were mostly confined to the dorsal part of the STN, with no significant difference between their median locations (Mann–Whitney U-test, $P > 0.1$). Non-oscillatory neurons were more evenly spread on the dorso-lateral STN axis, with a significantly different median from the HFB, TFB and DFB ones (Mann–Whitney U-test, $P < 0.001$). See also Supplementary Fig. 3 for details.

The analysis of single neuronal spike train oscillations cannot be easily extended to the continuous traces containing a mixture of recorded neurons and their background

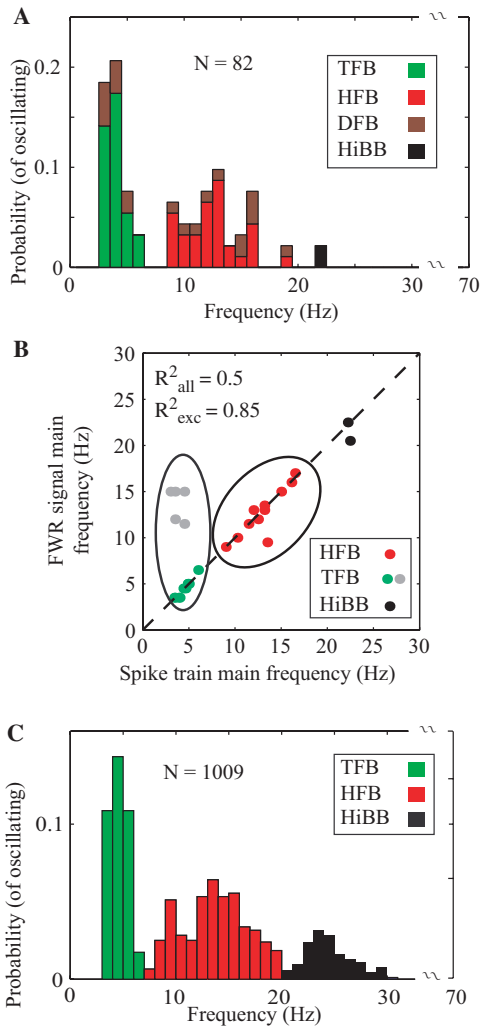

Fig. 4 Oscillation distribution in STN single and population neuronal activity. (**A**) Histogram of the main frequency of the oscillating neuronal spike trains, presented as a fraction of the total significantly oscillating neurons. (**B**) Relationship of the main frequency calculated for each neuron's FWR trace and its spike train. Ellipses surround the two neuron groups. TFB spike trains are divided into two subgroups according to the main frequency of their FWR trace: the TFB range (green) and the HFB range (grey). Dashed line indicates linear regression analysis to the identity line (forcing the slope to 1). R^2_{all}: including all neurons, R^2_{exc}: excluding the grey dots group. (**C**) FWR traces main frequency histogram, presented as a fraction of the total oscillating traces.

(multi-unit activity), since the former is a series of time-stamps while the latter is a continuously sampled filtered signal. However these traces may be analysed to reveal the spectral characteristics of significant oscillations in the multiunit domain. To do so, the FWR method was applied, enabling spectral evaluation of the signal's envelope (Fig. 1B). When the maximal peak frequency in the PSD of the spike trains and the FWR raw trace recorded on the same electrode were compared, they showed remarkable similarity (examples in Fig. 1C). At the oscillating neuronal population level this similarity is quantified by the deviation from the identity line of the maximal amplitude frequency of the spike train versus that of its FWR raw trace (Fig. 4B) yielding $R^2_{all} = 0.5$ $P < 0.001$. While most of the neurons were aligned on the diagonal, a small group of TFB neurons (7 of 37, 18% of TFBs) had a FWR trace main oscillation in the higher band, suggesting a considerable contribution of HFB oscillation power from the neuronal background. Excluding this group resulted in an increased fit $R^2_{exc} = 0.85$, $P < 0.001$. The identity relationship of the single unit point process and the continuous sampled raw activity enabled the expansion of the analysis to sessions which contained multi-unit activity. A total of 2171 stable recording sessions were spectrally analysed using the FWR method, of which 1009 (46%) showed significant oscillatory activity. The distribution of the maximal amplitude frequency of the FWR signal (Fig. 4C) showed a tri-modal distribution with two peaks similar to the ones found in the spike train analysis (Fig. 4A), and another smaller peak at 24 Hz in the high beta band. The similarity between the results from the two different analysis techniques further strengthens the validity of the FWR method as a source of spectral multi-unit trace information. It also establishes the existence and validity of the two main (TFB and HFB) oscillation ranges.

Spectral characteristics of neuronal background activity

The high-pass filtered background activity of a neuron recorded extra-cellularly reflects the spiking activity of multiple surrounding neurons in this neuron's vicinity. Oscillations in this background activity suggest correlated synchronous oscillatory activity in the neuron's local surrounding population. To study the properties of this neuronal background activity separately from the main neuron spiking activity we replaced its spike locations in the raw traces of the 37 TFB and 34 HFB neurons (we excluded the DFB neurons from this analysis) with random consecutive non spike traces from the same recording session. This procedure produced background traces which were generally spike-free apart from occasional smaller secondary neuron spikes (Fig. 2).

The spectral characteristics of the FWR raw signals (Fig. 5A), FWR extracted background (Fig. 5B, blue) and their associated spike train were compared. Since these three signals have different total power, each of the PSDs was normalized by its total power between 3–70 Hz (Fig. 5C). This analysis resulted in a very different image of the two groups around their main oscillatory frequency: the TFB neuron exhibited high normalized power of the spike train and low, flat, normalized power of the background (Fig. 5C, left), whereas the HFB neuron was characterized by high normalized power of the background and lower power for the spike trains (Fig. 5C, right).

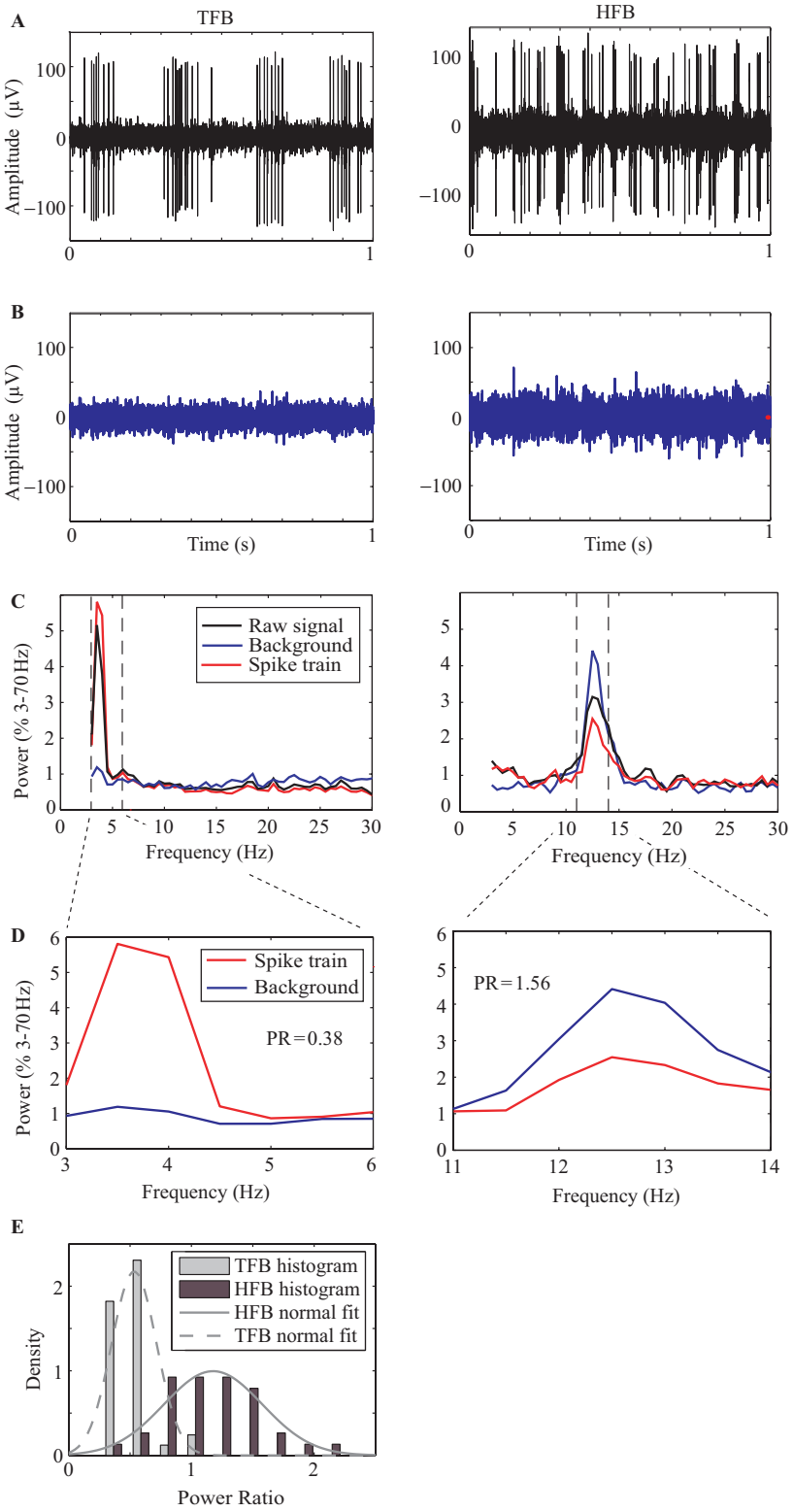

Fig. 5 Differences in spectral characteristics of background oscillatory activity between TFB and HFB groups. (**A**) Raw traces of TFB (left) and HFB (right) oscillating neurons. (**B**) Background activity of the traces in (**A**) after spike removal. (**C**) Normalized PSD of the FWR raw data (black), FWR background (blue) traces and spike train (red) normalized by the total power between 3 HZ and 70 Hz of each signal. The vertical dashed lines delimit the area around the spike train main frequency where the PR was calculated. (**D**) Enlarged view of the area where the PR index was calculated for the normalized PSDs in (**C**). The normalized power of the background (blue) was divided by that of the spike train (red) around the spike train main frequency. (**E**) PR distribution of TFB and HFB neurons groups. Dashed and continuous grey lines indicate normal fit for TFB and HFB group distributions, respectively.

The difference between the spike train and its background was quantified using the PR index. The PR index was calculated by dividing the normalized PSD of the FWR background trace by that of the spike train in a narrow 3 Hz band surrounding the main oscillatory frequency of the neuron (Fig. 5D). The index does not compare the actual powers, but rather the tendency to oscillate within the specific narrow band. Thus, a low PR of 0.38 for the TFB (Fig. 5D, left) suggests a lower tendency of the background to oscillate in the TFB band compared to that of the spiking activity. The same analysis for the HFB unit produces a high index of 1.56 (Fig. 5D, right), indicating a higher tendency of the background to oscillate in the main oscillatory frequency compared to the spiking activity. The PR distribution of the STN data presents two distinct, well-separated groups (Fig. 5E). The mean PR index of the HTB group (1.17 ± 0.07, mean $\pm$ SEM) was significantly larger than the TFB (0.53 ± 0.03, mean $\pm$ SEM) group (unpaired student *t*-test, $P < 0.001$).

Coherence of units and background oscillations

The correlation between neuronal spiking activity and the background oscillation activity in the frequency domain was analysed using a coherence measure which normalizes the cross-spectrum of two signals by dividing by both auto-spectrums (Fig. 6A). Coherence significance was tested for frequencies in the 3 Hz band surrounding the neuron spike train's main oscillatory frequency (Fig. 6B). Significant coherence was found in only half of the TFB neurons (18/37, 48%), compared to all of the HFB neurons (34/34, 100%) (Fig. 6C).

Studying the spectral properties of the DFB group revealed that although these neurons had significant oscillatory activity in both frequency ranges of TFB and HFB, they displayed different coherence properties. Of the nine neurons in the DFB group only one (1/9, 11%) was coherent with the background in the TFB range while all (9/9, 100%) had significant coherence in the HFB range.

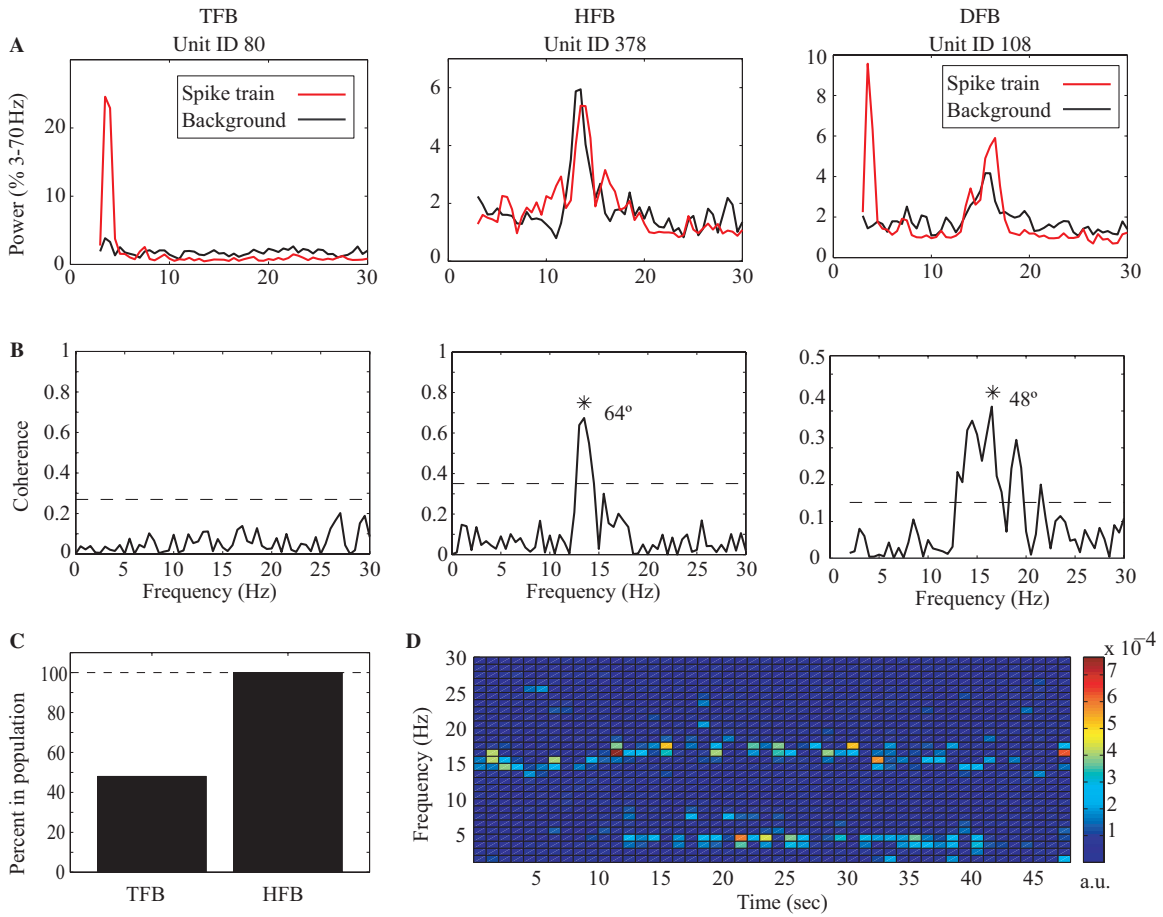

Fig. 6 Significant coherence between spike trains and their background activity in the HFB and TFB neuronal groups. (**A**) Normalized PSD of spike trains (red) and their FWR background (black) in examples of TFB (left), HFB (middle) and DFB (right) neurons. (**B**) Coherence between units and their FWR background activity in (**A**). Dashed line indicates $P < 0.01$ significance level. Asterisk indicates significant coherence in the spike train main frequency. The phase difference in degrees appears next to the peak frequency. (**C**) Percentage of TFB and HFB neurons which significantly oscillate coherently with their background. (**D**) Spectrogram of a DFB neuron. The neuron oscillates simultaneously in both frequency ranges. The spectral resolution is 1 Hz and time resolution is 1 s. a.u. = arbitrary units).

The time spans in which DFB neurons oscillated in the HFB and TFB frequency ranges were not mutually exclusive, i.e. a DFB neuron could oscillate simultaneously in both ranges (Fig. 6D).

Phase relation of spikes and background oscillations

Although all HFB and some TFB neurons were found to oscillate coherently with their background, their relative phases may vary; i.e. spikes can occur before, during, or after the oscillatory peak activity of its background. To assess the spike train phase distribution, the spikes were located on the band-passed filtered FWR oscillating background (Fig. 3A and B, before and after filtering). The FWR background was filtered with filter parameters allowing only the corresponding range to pass (i.e. 3–7 Hz and 8–20 Hz frequency ranges for HFB and TFB neurons, respectively). This method was favoured because both spikes and background display small cycle deviations which make standard methods such as cross-spectrum analysis less appropriate. For each neuron the spike phase distribution histogram was constructed and its deviation from circular uniform distribution was subjected to Rayleigh's test at $P<0.001$. For the neurons that passed the non-uniformity distribution test the mean phase and the cosine fitted phase were calculated (see 'Methods' section).

All (34/34) HFB neurons showed a significant deviation from uniformity of phase distribution compared to only 51% (19/37) of the TFB neurons (examples, Fig. 7A–C, see also Supplementary Fig. 2). The distribution of both the mean phase and the cosine-fitted θ phase found in the HFB neuron population displayed a narrow spread and showed a tendency to fire in close proximity and prior to the background oscillatory peak (Fig. 7D, see also Fig. 1A right and Fig. 5A right for traces exhibiting this phenomenon). Significant non-uniformly distributed TFB neuron phases showed a much wider distribution covering almost the whole phase spectrum (Fig. 7E). The mean and standard deviation of HFB neurons phase distributions were 155 ± 11 and 150 ± 11 for the mean phase and cosine fit, respectively, which translates to about 6 ± 2.5 ms before background peak activity for a 13 Hz oscillating neuron. Significant non-uniform phase TFB neurons had means of 184 ± 42 and 187 ± 58 for the mean phase and cosine fit, respectively, which translates to about 4 ± 34 ms after TFB background peak activity for a 4 Hz oscillating background. No significant differences were found between the two phase-analysis methods (*t*-test, $P<0.001$).

Temporal characteristics of TFB and HFB oscillations

Further differences between neurons belonging to the HFB and TFB groups were observed in the duration and continuity of oscillatory activity in the recorded sessions. This emerged from spectrogram analysis of both spike trains and FWR raw traces which allows for the inspection of the instantaneous PSD of the signals along the time axis. Signal duration was not significantly different between TFB and HFB signals (whether spike trains or raw FWR signals). However, TFB neural spike trains exhibited sparser, more sporadic oscillations compared to the continuous oscillatory nature of the HFB neurons (Fig. 8A). The same phenomenon was observed when looking at the spectrogram of the FWR raw traces from which both spike-trains in Fig. 8A were extracted (Fig. 8B).

To compare the oscillation duration and continuity of the two neuron populations, we calculated the percentage of non-overlapping one second windows in which the spike-train or FWR traces crossed a power threshold. We found a significant difference between the two groups (Fig. 8C); HFB neurons were found to fire in oscillation for longer periods of total spike train time (0.55 ± 0.06, mean ± SEM) than the TFB group (0.35 ± 0.03, mean ± SEM) (unpaired *t*-test $P<0.001$). We tested this phenomenon in the multiunit domain using the same analysis in long (longer than 30 s) and stable FWR raw recorded traces. The same significant difference in oscillatory duration was also found between 144 TFB and 154 HFB multi-unit traces (0.41 ± 0.02 and 0.28 ± 0.01, mean ± SEM for HFB and TFB, respectively) (Fig. 8D). Overall, these results show a more sporadic, transient oscillation period pattern for TFB neurons compared to the continuous oscillation of HFB neurons.

Discussion

Key physiological characteristics of the parkinsonian state are the emergence of neuronal oscillations in the basal ganglia (Bergman *et al.*, 1994; Raz *et al.*, 2000; Brown *et al.*, 2001; Cassidy *et al.*, 2002; Levy *et al.*, 2002*b*; Priori *et al.*, 2002) and an increase in synchronous neuronal firing in these nuclei (Raz *et al.*, 1996; Levy *et al.*, 2000; Hammond *et al.*, 2007). This study analyses the link between these two phenomena in human patients by studying STN neuronal oscillations and their relationship to synchronized oscillations in their surrounding local population depicted by their background activity. We found two major groups of oscillating neurons, the TFB and HFB groups, which could be differentiated by their frequency of oscillating activity. By using oscillations in the background activity of these neurons as a marker for synchronous activity in the local neuronal population we found that these neural groups also differ with respect to the characteristics of their neighbouring neurons. The HFB neurons are part of a more continuously activated, synchronous, oscillating local population, while the TFB neurons generally oscillate individually, and are locally surrounded by non-oscillating neurons and/or a population of out-of-phase neurons. We also showed that all HFB neurons oscillate coherently with their neighbouring population while only half did so in the

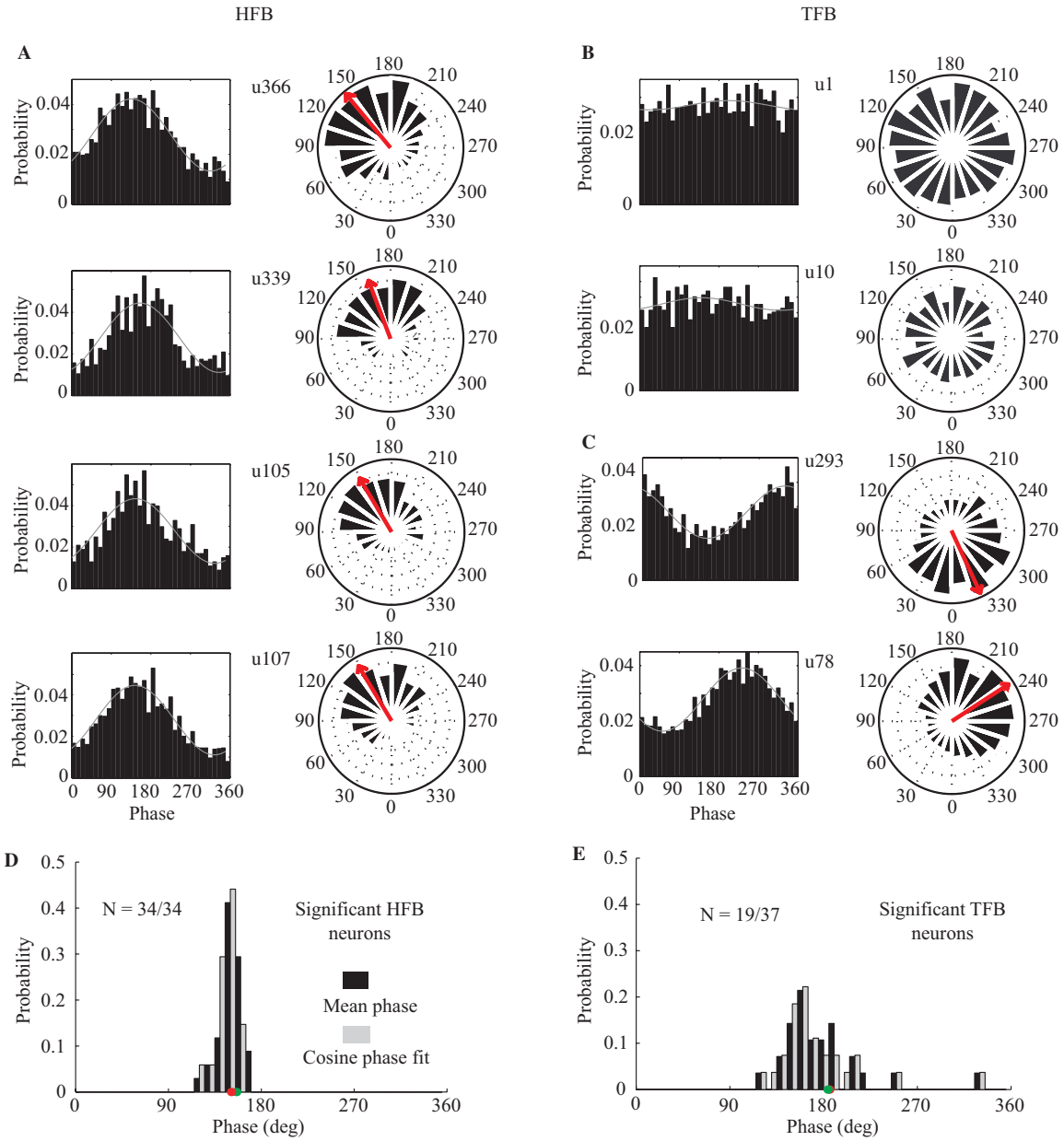

Fig. 7 Differences in HFB and TFB neuron spike phase distributions. Examples of 4 HFB and 4 TFB single neuron phase distributions, presented in bar and circular plots. The grey line on the bar graphs indicates the cosine fit to the distribution. The red arrow indicates the mean phase and appears only when the distribution deviated significantly ($P < 0.001$) from the uniform distribution using a Rayleigh test. (**A**) Four HFB neurons show significant deviation from the uniform distribution with a narrow population mean distribution as indicated by the common general direction of all red arrows shown. (**B**) Two illustrative neurons with no significant deviation from the uniform distribution of the TFB neuronal population. (**C**) Two examples of TFB neurons with significant deviation from the uniform distribution, each with a mean phase pointing to a different quarter of the unit cycle. (**D** and **E**) Mean (black) and cosine fit (grey) distributions of phases between spikes and band-passed filtered background of HFB and TFB neuronal populations. Green and red dots at zero level indicate the means of cosine fit and mean phase distributions, respectively. (**D**) Significant non-uniform phase distributed HFB neurons. (**E**) Significant non-uniform phase distributed TFB neurons.

TFB group. These results are inline with previous studies showing pair-wise coherence in the beta band compared to no coherency in the tremor band of pairs of STN neurons (Levy *et al*.. 2000). Altogether, these results suggest a different local functional organization of the two main groups of oscillating neurons. The co-activation of the HFB neuronal local population and the more isolated oscillatory activity of the TFB neurons may play different roles in the clinical manifestation of the parkinsonian state.

The different oscillating groups displayed similar properties in their localization and firing rate while maintaining a difference from non-oscillating neurons. The dorso-ventral

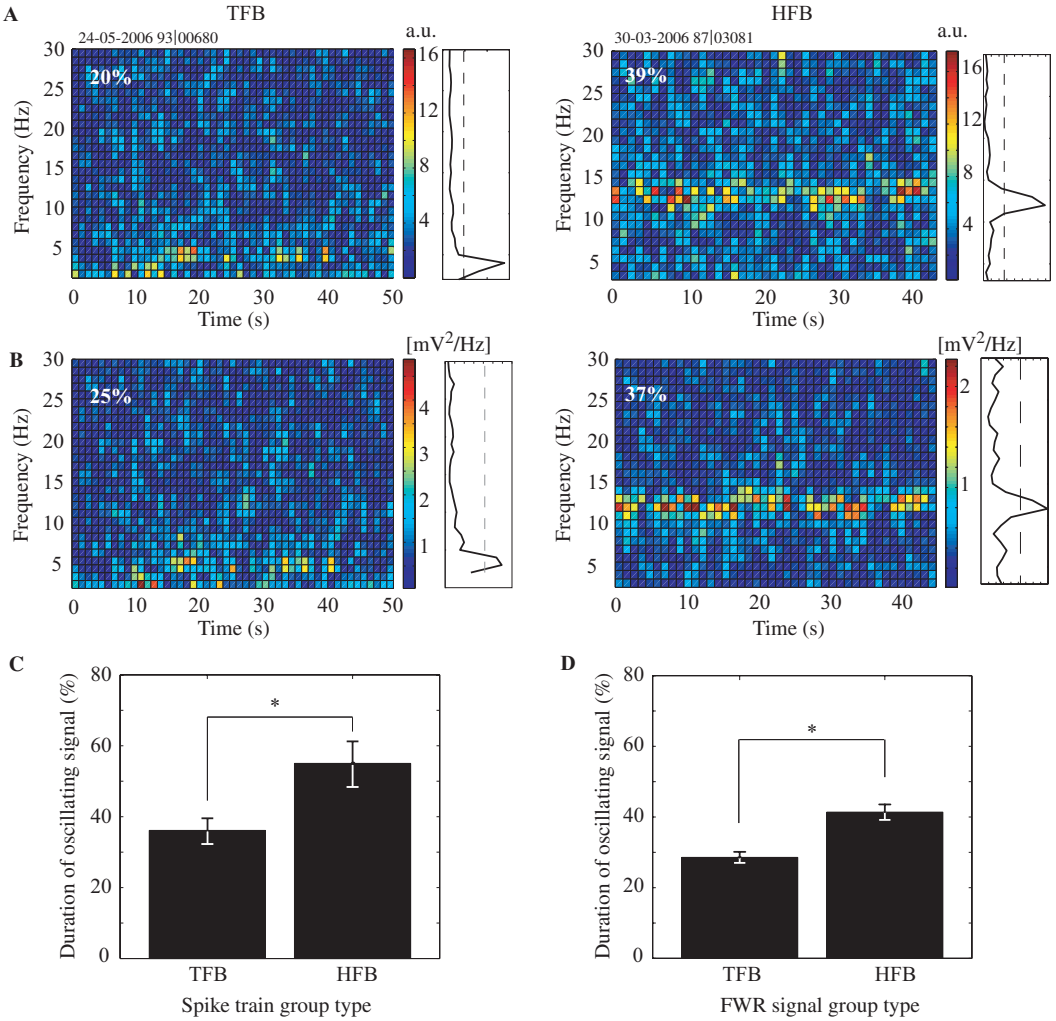

Fig. 8 Longer oscillation duration of HFBs compared with TFBs neurons and FWR signals. Spectrogram representations of time-frequency domains of spike trains and their FWR traces, for TFB (left) and HFB (right) groups, with the calculated percent significant oscillation duration for each signal in the upper left corner. The corresponding PSD of each spectrogram is presented to its right. (**A**) Spike train spectrograms. (**B**) Spectrograms of the FWR raw traces from which the spike trains in (**A**) were extracted. (**C**) Difference in mean oscillation time period for HFB and TFB neuron groups. HFB neurons oscillate for significantly longer periods than TFB neurons (unpaired student *t*-test $P < 0.01$). (**D**) Difference in mean oscillation time period of 30 s multi-unit signals of 144 TFB and 141 HFB. Signals with maximal frequency in the HFB band oscillate significantly longer than those with maximal frequency in the TFB band (unpaired student *t*-test $P < 0.001$). a.u. = arbitrary units.

macro-organization of the recordings reveals co-localization of all oscillating groups in the dorsal half, the sensory-motor part of the STN (Parent and Hazrati 1995), giving further support to their role in the motor impairments of Parkinson's disease. This contrasts with the uniform distribution of non-oscillating neurons. Firing rate was also found to be similar between all oscillating neuronal groups, but was significantly higher than the non-oscillating neurons, which is consistent with previous studies (Bergman *et al.*, 1994; Levy *et al.*, 2000).

A major difference between the TFB and the HFB neuronal groups was found in their multi-unit background oscillation. Since the recorded traces used as substrate for background reconstruction are high pass filtered over 250 Hz (to overcome the noisy electrical environment of the hospital operating room), they are the sum of fast changing potentials in the extra-cellular medium, and therefore are mainly influenced by spikes of nearby neurons. Like the Hilbert transform which is a common envelope extraction technique, the FWR technique allows for estimation of the low-frequency modulation (the signal's envelope) of this high-frequency activity (Journee, 1983; Myers *et al.*, 2003). The cumulative multi-unit spiking activity is functionally different from the LFPs recorded in other studies although both inspect the same frequency ranges. LFP is believed to mainly reflect slow sub-threshold currents, primarily post-synaptic potentials, of a large neuronal population from a radius of several millimetres (Ecceles, 1951) and are considered to be mainly the 'input' to the local network (Logothetis, 2002). In our

high-passed filtered recorded traces these slow, low-frequency modulations are filtered out, leaving only the high-frequency modulations that primarily reflect the spiking activity which is the 'output' of the network. In contrast to the low-frequency LFP signals which decay over a distance of several millimetres, the high-frequency signals resulting from action potentials decay over significantly shorter distances. According to a spike decay analysis in extra-cellular fluid (Rall, 1962) a 300 μV amplitude extra-cellular spike will decay into the 100 μV background within a distance of 2–3 soma radii. In the human STN this extends to no more than 100 microns which populate no more than 10 neurons (Hardman *et al.*, 2002).

Previous studies have reported the existence of high beta band (20–30 Hz) oscillations in the STN both in spike trains (Levy *et al.*, 2000; Weinberger *et al.*, 2006) and LFP (Brown *et al.*, 2001; Cassidy *et al.*, 2002; Priori *et al.*, 2004). In our study, only a negligible minority (2/231, 0.8%) of single neuron spike trains were found to oscillate in this band. This difference may be the outcome of a more stringent definition of the significance limit. The difference of our results from the results of the LFP studies may be explained by the different population sizes mentioned before or the low-pass filtering properties of the post-synaptic units (Fortune and Rose, 1997). However, we cannot rule out the possible existence of a distinct neuronal population with HiBB oscillations in a large neuronal sample. A possible hint to their existence may be reflected in the third spectral peak of the FWR raw signals (Fig. 4C).

Network summations of oscillations are apparent only when the neurons oscillate coherently with each other; otherwise their oscillations cancel each other out and produce a flat power spectrum. In this study, coherence analysis between all HFB oscillating neurons and their background manifested constructive in-phase coherent oscillation in the neuron's main frequency. Thus we expected to see a narrow phase distribution around zero when investigating the phase between HFB neurons and their oscillating background. The phase was in fact normally distributed near zero, but with a phase shift equivalent to about 6 ms prior to the background activity peak. Had the oscillating background been the outcome of dendritic input to the local population we would have expected it to precede the spike train oscillation, but our data proved otherwise.

How do these local populations synchronize? Anatomical studies have shown sparse interconnectivity in the STN (Sato *et al.*, 2000). However, modelling studies have shown that such sparse interconnectivity which leads to weak correlations at the pair-wise neuronal level can still lead to strong correlation at the network level (Schneidman *et al.*, 2006). Furthermore, the synchrony may be generated in other, well interconnected regions such as the cortex (Abeles, 1991; Goldberg *et al.*, 2004), which later could impose this synchronized oscillation on downstream areas such as the STN.

Overall, our results suggest that the local co-activity properties of the two neuronal groups are different.

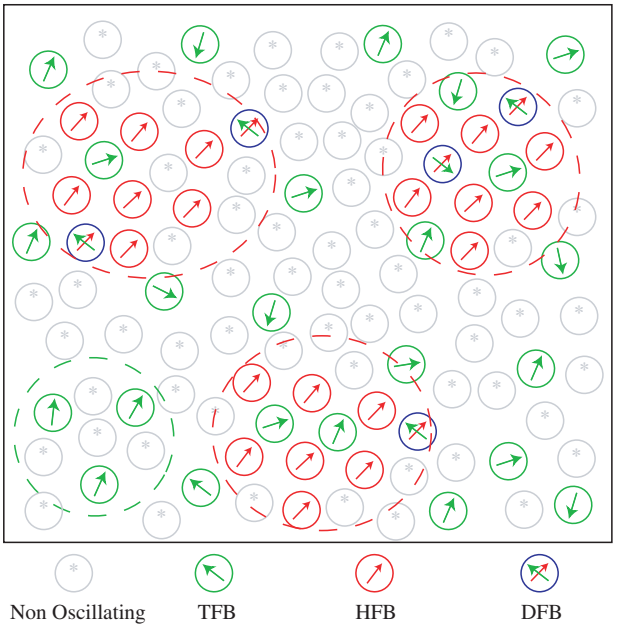

Fig. 9 Functional organization model of the STN. Red and green circled arrows represent HFB and TFB neurons, respectively. Blue circled red and green arrows represent DFB neurons. Grey circled asterisks represent non-oscillatory neurons. Arrow direction represents the oscillation phase. HFB neurons are clustered in patches (red dashed ellipses) and share a common phase. TFB neurons are more evenly spread and usually do not share a common phase with their TFB neighbours, apart from occasional territories with a common phase (green dashed ellipse). DFB neurons are located in HFB neuronal patches and share its common phase, while its TFB oscillation phase is not necessarily identical to nearby TFB neurons.

The HFB neurons seem to be part of a more synchronized, coherently oscillating local population, with longer periods of continuous oscillatory activity. On the other hand, the TFB neuronal non-oscillatory background is probably the outcome of a local population that is a mixture of non-oscillatory neurons and several out-of-phase TFB neurons (Levy *et al.*, 2000). Our data are summarized in the functional organization model (Fig. 9). In this model HFB neurons are clustered in specific regions, and share a common phase. This common phase leads to the high coherence with its background in the HFB range. TFB neurons, on the other hand, are spread more evenly but typically do not share a common phase with their TFB neighbours. This leads to the flat power and non-coherent TFB background. In certain restricted areas several TFB neurons share a close phase leading to significant coherence with the measured background. DFB neurons fit this model by being influenced by the two drives within the HFB patches. Since this area is modelled to contain a population of in-phase HFB neurons, out-of-phase TFB neurons and non-oscillatory neurons, it corresponds to our result that significant coherence is almost always found only with the background in the HFB frequency range.

Analysis of the relationship between the two neuronal populations and the clinical data did not reveal significant

differences between the mean clinical scores of rigidity, tremor or bradykinesia when trying to subgroup the patient population according to their cells type content. However, since the number of cells per patient is very small in this study, the division of the patients into subgroups may be biased; therefore we cannot rule out the possibility of a relationship between cell type prevalence and clinical state. For the same reason the almost equal number of HFBs and TFBs found in this study should not lead to any conclusion regarding the prevalence of the two populations within a single patient.

The high-frequency synchronous HFB oscillatory activity produces a considerable driving force to downstream targets which should be detected by EMG if the information is linearly transformed in the pathways from the basal ganglia through the thalamus to the cortex and downstream to the muscles. As the HFB oscillation range is manifested by tremor in other neurological diseases such as essential tremor (Deuschl *et al.*, 2001), its paucity in the extremity EMG of Parkinson's disease patients at rest is puzzling [although its lower bound may also be found in the Parkinson's disease action tremor (Lance *et al.*, 1963)]. A recent study described low-pass filtering properties of the cortex-periphery pathways with a cut-off frequency at around 5 Hz (Lalo *et al.*, 2008; Rivlin-Etzion *et al.*, 2008). This finding might explain why the high-frequency bursting activity that we found does not propagate to the patients' extremities. Another explanation follows anatomical studies that have found that much of the output of the basal ganglia reaches the frontal cortex such as the pre-motor and supplementary motor areas (Schell and Strick, 1984). It is, therefore, possible that the HFB oscillations do not reach motor areas directly but rather interrupt higher goal directing, or movement planning regions, leading to hypokinetic clinical symptoms such as akinesia and bradykinesia. This hypothesis is strengthened by our finding that HFB neurons tend to fire in a more continuous manner than the sporadic oscillation pattern of TFB neurons. In terms of clinical symptoms it is appealing to associate the TFB activity with the transient and uncorrelated nature of Parkinson's disease peripheral tremor (Raethjen *et al.*, 2000; Ben-Pazi *et al.*, 2001), which shares the TFB frequency range, and the HFB neuronal activity to the continuous hypokinetic Parkinson's disease state.

Supplementary material

Supplementary material is available at *Brain* online. Software related to this article can be downloaded from http://neurint.ls.biu.ac.il

Acknowledgements

We thank Tami Muller for her assistance with the patients' clinical data and Rony Paz for his helpful comments.

Funding

The Israel Science Foundation (ISF-1000-05 to I.B.); the Ministry of Health (MOH-3-4033 to I.B.); and 'Fighting against Parkinson' grant (to H.B.) administrated by the Netherlands Friends of the Hebrew University (HUNA).

References

Abeles M. Corticonics, neural circuits of the cerebral cortex. Cambridge: Cambridge University press; 1991.

Alexander GE, Crutcher MD. Functional architecture of basal ganglia circuits: neural substrates of parallel processing. Trends Neurosci 1990; 13: 266–71.

Alexander GE, DeLong MR, Strick PL. Parallel organization of functionally segregated circuits linking basal ganglia and cortex. Annu Rev Neurosci 1986; 9: 357–81.

Amirnovin R, Williams ZM, Cosgrove GR, Eskandar EN. Visually guided movements suppress subthalamic oscillations in Parkinson's disease patients. J Neurosci 2004; 24: 11302–06.

Amtage F, Henschel K, Schelter Br, Vesper J, Lücking CH, Hellwig B. Tremor-correlated neuronal activity in the subthalamic nucleus of Parkinsonian patients. Neurosci Lett 2008; 442: 195–9.

Ben-Pazi H, Bergman H, Goldberg JA, Giladi N, Hansel D, Reches A, Simon ES. Synchrony of rest tremor in multiple limbs in parkinson's disease: evidence for multiple oscillators. J Neural Transm 2001; 108: 287–96.

Bergman H, Wichmann T, Karmon B, DeLong MR. The primate subthalamic nucleus. II. Neuronal activity in the MPTP model of parkinsonism. J Neurophysiol 1994; 72: 507–20.

Brown P, Oliviero A, Mazzone P, Insola A, Tonali P, Di Lazzaro V. Dopamine dependency of oscillations between subthalamic nucleus and pallidum in Parkinson's disease. J Neurosci 2001; 21: 1033–8.

Buzsaki G. Rhythms of the brain. Oxford: Oxford University Press; 2006.

Cassidy M, Mazzone P, Oliviero A, Insola A, Tonali P, Di Lazzaro V, Brown P. Movement-related changes in synchronization in the human basal ganglia. Brain 2002; 125: 1235–46.

Deuschl G, Raethjen J, Lindemann M, Krack P. The pathophysiology of tremor. Muscle Nerve 2001; 24: 716–35.

Drouot X, Oshino S, Jarraya B, Besret L, Kishima H, Remy P, et al. Functional recovery in a primate model of Parkinson's disease following motor cortex stimulation. Neuron 2004; 44: 769–78.

Ecceles JC. Interpretation of action potentials evoked in the cerebral cortex. Electroencephalogr Clin Neurophysiol 1951; 3: 449–64.

Engel AK, Fries P, Konig P, Brecht M, Singer W. Temporal binding, binocular rivalry, and consciousness. Conscious Cogn 1999; 8: 128–51.

Fee MS, Mitra PP, Kleinfeld D. Variability of extracellular spike waveforms of cortical neurons. J Neurophysiol 1996; 76: 3823–33.

Fortune ES, Rose GJ. Passive and active membrane properties contribute to the temporal filtering properties of midbrain neurons in vivo. J Neurosci 1997; 17: 3815–25.

Goldberg JA, Rokni U, Boraud T, Vaadia E, Bergman H. Spike synchronization in the cortex/basal-ganglia networks of Parkinsonian primates reflects global dynamics of the local field potentials. J Neurosci 2004; 24: 6003–10.

Gourevitch B, Eggermont JJ. A simple indicator of nonstationarity of firing rate in spike trains. J Neurosci Methods 2007; 163: 181–7.

Hammond C, Bergman H, Brown P. Pathological synchronization in Parkinson's disease: networks, models and treatments. Trends Neurosci 2007; 30: 357–64.

Hardman CD, Henderson JM, Finkelstein DI, Horne MK, Paxinos G, Halliday GM. Comparison of the basal ganglia in rats, marmosets, macaques, baboons, and humans: volume and neuronal number for the output, internal relay, and striatal modulating nuclei. J Comp Neurol 2002; 445: 238–55.

Heimer G, Bar-Gad I, Goldberg JA, Bergman H. Dopamine replacement therapy reverses abnormal synchronization of pallidal neurons in the 1-methyl-4-phenyl-1,2,3,6-tetrahydropyridine primate model of Parkinsonism. J Neurosci 2002; 22: 7850–5.

Hurtado JM, Rubchinsky LL, Sigvardt KA, Wheelock VL, Pappas CT. Temporal evolution of oscillations and synchrony in GPi/muscle pairs in Parkinson's disease. J Neurophysiol 2005; 93: 1569–84.

Hutchison WD, Lozano AM, Tasker RR, Lang AE, Dostrovsky JO. Identification and characterization of neurons with tremor-frequency activity in human globus pallidus. Exp Brain Res 1997; 113: 557–63.

Journee HL. Demodulation of amplitude modulated noise: a mathematical evaluation of a demodulator for pathological tremor EMG's. biomedical engineering, IEEE transactions on 1983; BME-30: 304–8.

Kuhn AA, Williams D, Kupsch A, Limousin P, Hariz M, Schneider GH, et al. Event-related beta desynchronization in human subthalamic nucleus correlates with motor performance. Brain 2004; 127: 735–46.

Lalo E, Thobois S, Sharott A, Polo G, Mertens P, Pogosyan A, et al. Patterns of bidirectional communication between cortex and basal ganglia during movement in patients with Parkinson disease. J Neurosci 2008; 28: 3008–16.

Lance JW, Schwa RS, Peterson EA. Action tremor and the cogwheel phenomenon in Parkinson's disease. Brain 1963; 86: 95–110.

Lang AE, Widner H. Deep brain stimulation for Parkinson's disease: patient selection and evaluation. Mov Disord 2002; 17 (Suppl 3): S94–101.

Lemstra AW, Verhagen Metman L, Lee JI, Dougherty PM, Lenz FA. Tremor-frequency (3-6 Hz) activity in the sensorimotor arm representation of the internal segment of the globus pallidus in patients with Parkinson's disease. Neurosci Lett 1999; 267: 129–32.

Lenz FA, Tasker RR, Kwan HC, Schnider S, Kwong R, Murayama Y, et al. Single unit analysis of the human ventral thalamic nuclear group: correlation of thalamic "tremor cells" with the 3-6 Hz component of parkinsonian tremor. J Neurosci 1988; 8: 754–64.

Levy R, Ashby P, Hutchison WD, Lang AE, Lozano AM, Dostrovsky JO. Dependence of subthalamic nucleus oscillations on movement and dopamine in Parkinson's disease. Brain 2002a; 125: 1196–209.

Levy R, Dostrovsky JO, Lang AE, Sime E, Hutchison WD, Lozano AM. Effects of apomorphine on subthalamic nucleus and globus pallidus internus neurons in patients with Parkinson's disease. J Neurophysiol 2001; 86: 249–60.

Levy R, Hutchison WD, Lozano AM, Dostrovsky JO. High-frequency synchronization of neuronal activity in the subthalamic nucleus of parkinsonian patients with limb tremor. J Neurosci 2000; 20: 7766–75.

Levy R, Hutchison WD, Lozano AM, Dostrovsky JO. Synchronized neuronal discharge in the basal ganglia of parkinsonian patients is limited to oscillatory activity. J Neurosci 2002b; 22: 2855–61.

Logothetis NK. The neural basis of the blood-oxygen-level-dependent functional magnetic resonance imaging signal. Philos Trans R Soc Lond B Biol Sci 2002; 357: 1003–37.

Machado A, Rezai AR, Kopell BH, Gross RE, Sharan AD, Benabid AL. Deep brain stimulation for Parkinson's disease: surgical technique and perioperative management. Mov Disord 2006; 21 (Suppl 14): S247–58.

Middleton FA, Strick PL. Basal-ganglia 'Projections' to the prefrontal cortex of the primate. Cereb Cortex 2002; 12: 926–35.

Mink JW. The basal ganglia: focused selection and inhibition of competing motor programs. Prog Neurobiol 1996; 50: 381–425.

Moran A, Bar-Gad I, Bergman H, Israel Z. Real-time refinement of subthalamic nucleus targeting using Bayesian decision-making on the root mean square measure. Mov Disord 2006; 21: 1425–31.

Myers LJ, Lowery M, O'Malley M, Vaughan CL, Heneghan C, St Clari GA, et al. Rectification and non-linear pre-processing of EMG signals for cortico-muscular analysis. J Neurosci Methods 2003; 124: 157–65.

Pare D, Collins DR, Pelletier JG. Amygdala oscillations and the consolidation of emotional memories. Trends Cogn Sci 2002; 6: 306–14.

Parent A, Hazrati LN. Functional anatomy of the basal ganglia. II. The place of subthalamic nucleus and external pallidum in basal ganglia circuitry. Brain Res Brain Res Rev 1995; 20: 128–54.

Pessiglione M, Guehl D, Rolland AS, Francois C, Hirsch EC, Feger J, et al. Thalamic neuronal activity in dopamine-depleted primates: evidence for a loss of functional segregation within basal ganglia circuits. J Neurosci 2005; 25: 1523–31.

Priori A, Foffani G, Pesenti A, Bianchi A, Chiesa V, Baselli G, et al. Movement-related modulation of neural activity in human basal ganglia and its L-DOPA dependency: recordings from deep brain stimulation electrodes in patients with Parkinson's disease. Neurol Sci 2002; 23 (Suppl 2): S101–2.

Priori A, Foffani G, Pesenti A, Tamma F, Bianchi AM, Pellegrini M, et al. Rhythm-specific pharmacological modulation of subthalamic activity in Parkinson's disease. Exp Neurol 2004; 189: 369–79.

Raethjen J, Lindemann M, Schmaljohann H, Wenzelburger R, Pfister G, Deuschl G. Multiple oscillators are causing parkinsonian and essential tremor. Mov Disord 2000; 15: 84–94.

Rall P. Electrophysiology of a dendritic neuron model. Biophys J 1962; 2: 145–67.

Raz A, Feingold A, Zelanskaya V, Vaadia E, Bergman H. Neuronal synchronization of tonically active neurons in the striatum of normal and parkinsonian primates. J Neurophysiol 1996; 76: 2083–8.

Raz A, Vaadia E, Bergman H. Firing patterns and correlations of spontaneous discharge of pallidal neurons in the normal and the tremulous 1-methyl-4-phenyl-1,2,3,6-tetrahydropyridine vervet model of parkinsonism. J Neurosci 2000; 20: 8559–71.

Rivlin-Etzion M, Marmor O, Saban G, Rosin B, Haber SN, Vaadia E, et al. Low-pass filter properties of basal ganglia cortical muscle loops in the normal and MPTP primate model of Parkinsonism. J Neurosci 2008; 28: 633–49.

Rosenberg JR, Amjad AM, Breeze P, Brillinger DR, Halliday DM. The Fourier approach to the identification of functional coupling between neuronal spike trains. Prog Biophys Mol Biol 1989; 53: 1–31.

Sanger TD. Theoretical considerations for the analysis of population coding in motor cortex. Neur Comput 1994; 6: 29–37.

Sato F, Parent M, Levesque M, Parent A. Axonal branching pattern of neurons of the subthalamic nucleus in primates. J Comp Neurol 2000; 424: 142–52.

Schell GR, Strick PL. The origin of thalamic inputs to the arcuate premotor and supplementary motor areas. J Neurosci 1984; 4: 539–60.

Schneidman E, Berry MJ, Segev R, Bialek W. Weak pairwise correlations imply strongly correlated network states in a neural population. Nature 2006; 440: 1007–12.

Schwab RS, Cobb S. Simultaneous electromyograms and electroencephalograms in Paralysis Agitans. J Neurophysiol 1939; 2: 36–41.

Timmermann L, Gross J, Dirks M, Volkmann J, Freund HJ, Schnitzler A. The cerebral oscillatory network of parkinsonian resting tremor. Brain 2002; 126: 199–212.

Volkmann J, Joliot M, Mogilner A, Ioannides AA, Lado F, Fazzini E, et al. Central motor loop oscillations in parkinsonian resting tremor revealed by magnetoencephalography. Neurology 1996; 46: 1359–70.

Weinberger M, Mahant N, Hutchison WD, Lazano AM, Moro E, Hodaie M, et al. Beta oscillatory activity in the subthalamic nucleus and its relation to dopaminergic response in Parkinson's disease. J Neurophysiol 2006; 96: 3248–56.

Wingeier B, Tcheng T, Koop MM, Hill BC, Heit G, Bronte-Stewart HM. Intra-operative STN DBS attenuates the prominent beta rhythm in the STN in Parkinson's disease. Exp Neurol 2006; 197: 244–51.

Zirh TA, Lenz FA, Reich SG, Dougherty PM. Patterns of bursting occurring in thalamic cells during parkinsonian tremor. Neuroscience 1998; 83: 107–21.